Journal of Sound and Vibration (1998) **214**(2), 309–324
Article No. sv981562

MEASUREMENT AND SIMULATION OF LOW FREQUENCY IMPULSE NOISE AND GROUND VIBRATION FROM AIRBLASTS

L. R. HOLE*

University Courses on Svalbard (*UNIS*), *P.O. Box* 156, 9170 *Longyearbyen*, *Norway*

AND

A. M. KAYNIA AND C. MADSHUS

Norwegian Geotechnical Institute (*NGI*), *P.O. Box* 3930 *Ullevaal Hageby*, *N*-0806, *Oslo*, *Norway*

(*Received* 8 *October* 1997, *and in final form* 6 *February* 1998)

This paper presents numerical simulations of low frequency ground vibration and dynamic overpressure in air using two different numerical models. Analysis is based on actual recordings during blast tests at Haslemoen test site in Norway in June 1994. It is attempted to use the collected airblast-induced overpressures and ground vibrations in order to assess the applicability of the two models. The first model is a computer code which is based on a global representation of ground and atmospheric layers, a so-called Fast Field Program (FFP). A viscoelastic and a poroelastic version of this model is used. The second model is a two-dimensional *moving-load* formulation for the propagation of airblast over ground. The poroelastic FFP gives the most complete and realistic reproduction of the processes involved, including decay of peak overpressure amplitude and dominant frequency of signals with range. It turns out that the *moving-load* formulation does not provide a complete description of the physics involved when the speed of sound in air is different from the ground wavespeeds.

1. INTRODUCTION

This paper presents numerical simulations of ground vibration and dynamic overpressure in air at an instrumented test site at Haslemoen, Norway. The tests, which were performed in June 1994, were part of an extensive field test program entitled *Blast Propagation through Forest*. One of the objectives of this program has been to use collected data in order to verify existing noise/vibration prediction models and to identify potential improvements and modifications to such models. Two numerical formulations are tested out in this paper. The first one is based on a global representation of the ground and atmospheric (acoustic) layers, and the other is a 2-D formulation of layered media under moving-load. The results presented cover various analyses including waveform simulation and decay rate of peak values with distance.

Over the years, propagation of air-borne acoustic pulses above a flat and uniform ground has been studied by several authors with different approaches. Methods applied include complex impedance ground representation [1] a rigid-porous approximation [2],

* *E-mail:* larshole@unis.no.

0022–460X/98/270309 + 16 $30.00/0

or a viscoelastic approach [3]. Predictions of normalized overpressure waveforms in a homogeneous atmosphere, or of the peak pressure amplitudes in a refracting atmosphere have been studied separately. This paper presents calculations of overpressure waveforms, amplitudes and ground vibrations, using a more complete, poroelastic approach implemented in a Fast Field Program (FFP), OASES [4]. This new version of OASES has not been tested on atmospheric sound propagation problems before, but has shown promising results for propagation in water-saturated sand in the 10- to 100-kHz band [5]. The model can also handle a refracting atmosphere, but that is not considered here. A similar code has been used earlier to predict sound propagation at single frequencies, and the possible effect of ground elasticity on above ground sound propagation has been pointed out [6]. However, these results were not compared with experimental data. The theoretical results produced here are compared with viscoelastic FFP predictions, and with experimental data.

A different approach has also been tested out for the ground response to propagating airblast waves over ground. It is based on a *moving-load* formulation in which the atmospheric interaction is ignored and a steady state solution for ground vibration is determined [7]. A 2-D formulation of this type is used in this paper to compare with the more complete FFP model.

2. EXPERIMENT

2.1. TEST LAYOUT AND PROCEDURE

As part of a larger trial series, this experiment took place near Haslemoen army camp, 200 km north of Oslo, Norway, in June 1994. Only a brief overview is given here, since these measurements are described more completely elsewhere [8, 9]. One kilogram of unconfined charges of C4 plastic explosive were used as sound sources. C4 has a TNT weight equivalent of 1·32 and most of the energy is contained below 100 Hz [10, 11]. Non-linear effects were present in a region close to the source. However, only propagation of blast waves in the linear region further out is considered here.

The measurement set-up compared five microphones to measure the impulse noise and three seismometers (one horizontal and two vertical) to measure ground vibration. Two of the microphones were installed on a tall mast at elevations of 16 and 30 m above ground level and the other three were positioned on a shorter mast at elevations of 2, 4 and 8 m. Geophones and seismometers were installed in 0·75-m deep ditches close to the masts, but only surface data are presented here. The nominal frequency range of the microphones was 0·4 Hz to 8 kHz and that of the seismometers was 1 to 100 Hz. A total of 35 detonations were carried out in these blast test series. For each shot, 16 k data points of time histories of overpressures and ground particle velocity were recorded at a sampling rate of 10 kHz. For a detailed account of the tests and instrumentation see reference [12].

The experimental layout is shown in Figure 1. An open field of pasture land was situated next to a pine forest, with 18–25 m high trees, about 5 m apart. Both the pasture land and the forest ground was virtually flat and uniform. Charges were detonated along a straight line on a gravelled road along the edge of the forest, as shown in Figure 1. Detonation height was 2 m above ground. Thus, the blast waves propagated mostly through the forest. It is assumed that the trees hardly influence propagation of sound at the low frequencies considered here. Rather, the forest floor is of importance.

2.2. GROUND CONDITIONS

Ground conditions mostly decide the waveforms of the propagating airblast [2]. The relative importance of different ground parameters will be discussed in sections 3 and 5.

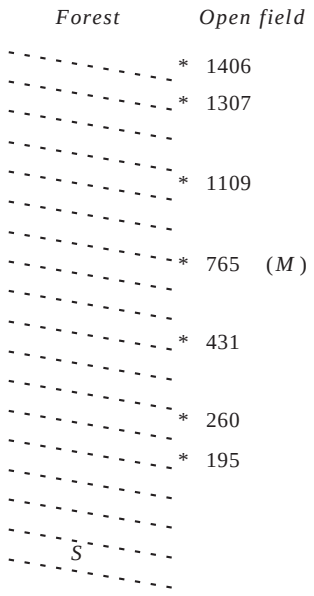

Figure 1. Plan view of the test site at Haslemoen. Shot points are indicated as asterisks (*), with distance to the receiver, *S* (South Station), in metres. *M* is the meteorological measuring point.

The soil profile at the site consists of a fairly uniform, 60-m deep layer of sandy silt overlying a rigid bedrock. A seismic survey was carried out by the *Spectral Analysis of Surface Waves* method [13, 14]. The resulting data are shown in Table 1. Poisson's ratio was estimated at 0·3 above water level and at 0·49 below. A moss layer about 0·3 m thick was present on top of the soil. For viscoelastic predictions, the data in Table 1 are sufficient, in addition to a value for ground attenuation of P- and S-waves. For poroelastic predictions, additional parameters must be included, as will be described in section 3.

2.3. METEOROLOGICAL CONDITIONS

A situation with rather stationary meteorological conditions and a weakly refracting atmosphere was selected for this analysis. Among other instruments, a Tethersonde was used to measure meteorological profiles up to 1000 m in the atmospheric boundary layer [15]. Examples of such profiles are shown in Figure 2 and support the assumption of stationary conditions during the test. Atmospheric refraction mostly affects the overpressure amplitude of the propagating wave [3] but is of less importance here. As will

TABLE 1

Ground data for Haslemoen. Layers 5 *and* 6 *were below ground water level*

Layer no.	Thickness (m)	Density (kg/m^3)	P wave-speed (m/s)	S wave-speed (m/s)
1	1	1500	250	130
2	1·5	1500	260	140
3	2·5	1500	280	150
4	5·0	1600	300	160
5	10·0	1700	1500	180
6	Half-space	1800	1500	250

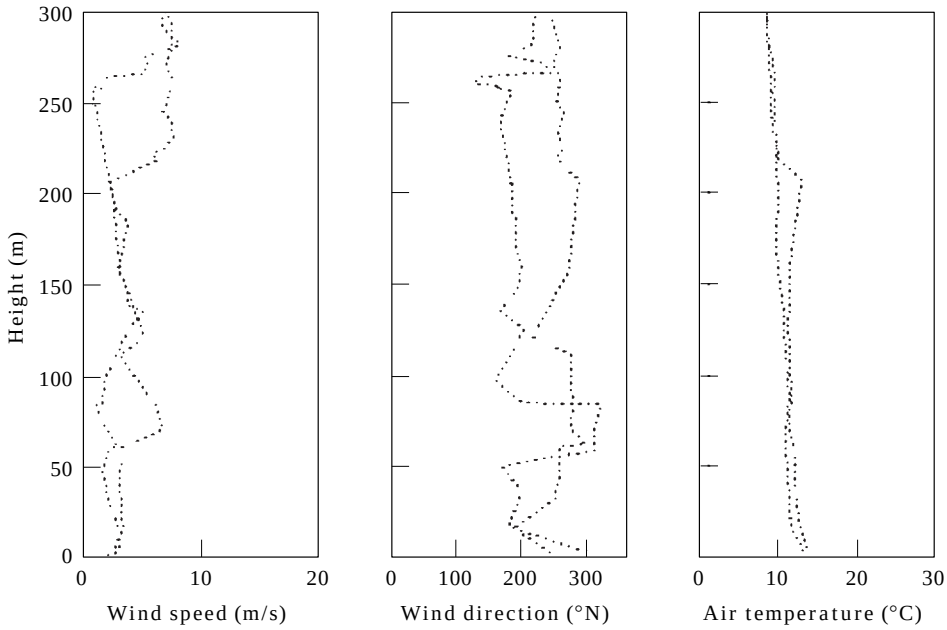

Figure 2. Meteorological profiles as measured by the Tethersonde June 15, 1414–1458. Both ascent and descent are shown.

be shown, predictions turn out to be satisfactory, even if a homogeneous atmosphere is assumed. The speed of sound, c, was set to 340 m/s in all calculations.

3. FFP MODEL

3.1. GENERAL

OASES [4] is a general purpose computer code for modelling the propagation of dynamic disturbances in a horizontally stratified system of viscoelastic or poroelastic solid and fluid layers. The model is essentially an upgraded version of the code SAFARI [16] which includes such enhancements as more efficient numerical integration, unconditional numerical stability, and incorporation of a poroelastic Biot model for the ground [17, 18]. It uses the closed-form solutions of wave propagation equations in a horizontally layered viscoelastic/poroelastic/acoustic system and, therefore, is by far the most efficient compared to traditional numerical techniques such as the finite difference method and the finite element method [16]. The rigorous handling of the infinite extent of the environment and the possibility of incorporating atmospheric layers are two appealing features of OASES. The aforementioned traditional techniques, however, provide flexibility in dealing with local inhomogeneities, topography and non-linear effects.

3.2. VISCOELASTIC VERSION

The viscoelastic version of OASES [4], is a well-known FFP model that does not need any detailed presentation. In this present application, a 2-D version was applied. Transfer functions are found at any receiver position for a selected number of frequencies. A post processor is provided to evaluate the frequency integral and map the solution into the time domain. Calculations presented here were integrated over the frequency interval from 0 to 100 Hz, with steps of 0·122 Hz. Further, minimum and maximum wave-speeds, c_{min} and

c_{max} (which decide the wavenumber integration interval), were set to 100 and 10^8 m/s, respectively. Other important parameters to decide are the number of time-points, set to 16 384, and the time-step, set to 0·0005 s. Thus, the time-window was about 8 s, which is sufficient for the ranges studied here. With these numerical parameters, solutions turned out to be numerically stable. In addition, the Filon integration scheme was applied. The transfer function was calculated for each 100 m, at 100–1400 m from the source. Linear interpolation was used to find the pulses at ranges corresponding to the measuring points. A standard normalized source pulse, shown in Figure 3, was applied. The central frequency was set to 30 Hz, which is close to the observed central frequency of these blasts [10]. Ground parameters as shown in Table 1 were included, in addition to an atmospheric sound speed, c of 340 m/s. Ground and atmospheric attenuation coefficients were set to 0·02 and 0·002 dB/wavelength, respectively. All pulses and particle velocities predicted by the viscoelastic FFP code were multiplied by a conversion factor of $2{\cdot}06 \times 10^4$, found by comparing measured and predicted peak overpressure amplitudes at 195 m from the source.

3.3. POROELASTIC VERSION

Even though a viscoelastic FFP model can be a useful tool to predict overpressure amplitudes [3], a more complete description of the ground is required to calculate accurate waveforms and ground particle velocities. A poroelastic Biot ground model [17, 18] has been included in OASES [4, 5], and the model allows for any combination of fluid layers and viscoelastic or poroelastic solid layers. Biot's model of a porous medium is based on the assumption that the medium consists of a viscoelastic solid frame completely filled with a fluid with density ρ_f and viscosity v. The theory differs from the viscoelastic approach in the way that it predicts one shear wave and two compressional waves. The shear wave (S) and the compressional wave of the first kind (P_1) travel mostly in the solid frame, while the compressional wave of the second kind (P_2) travels mostly through the pores. Thus, its speed is controlled by the fluid modulus. In the following, vector variables are written in bold types. Let $\mathbf{u}_s$ and $\mathbf{u}_f$ represent displacements of the solid frame and the fluid, and let indexes f and s indicate fluid and solid properties, respectively. Then $\mathbf{w} = \Omega(\mathbf{u}_s - \mathbf{u}_f)$ is the fluid displacement relative to the frame, where Ω is the porosity. Further, $e = \nabla \cdot \mathbf{u}_s$ is the volumetric strain of the solid and $\zeta = \nabla \cdot \mathbf{w}$ is the increment in fluid content. The

TABLE 2

List of Biot parameters included in poroelastic layer

Depth (m)	0·1, 0·3, 0·5 and 1·0
Density of pore fluid, ρ_f (kg/m^3)	1·2
Bulk modulus of pore fluid, K_f (10^6 Pa)	0·13
Pore fluid attenuation, δ_f (dB/wavelength)	0·002
Pore fluid dynamic viscosity, η (k/m · s)	$1{\cdot}74 \times 10^{-5}$
Solid grain density, ρ_s (kg/m^3)	2·7
Bulk modulus of solid grains, K_s (10^6 Pa)	9060
Sediment frame porosity, Ω	0·44
Sediment frame permeability, k_0 (10^{-10} m^2)	1, 10 and 100
Pore size factor, a (m)	10^{-3}
Sediment frame shear modulus, μ (10^6 Pa)	25·5
Sediment frame bulk modulus, K (10^6 Pa)	60·7
Shear and bulk attenuation, δ (dB/wavelength)	0·02
Tortuosity, α	1·25

average density of the fluid-saturated skeleton is, $\rho = \Omega\rho_f + (1 - \Omega)\rho_s$. Biot's equations of motion can be written as [5, 19],

$$\mu\nabla^2\mathbf{u}_s + (H - \mu)\nabla e - C\nabla\zeta = \rho\ddot{\mathbf{u}}_s - \rho_f\ddot{\mathbf{w}},$$
$$C\nabla e - M\nabla\zeta = \rho_f\ddot{\mathbf{u}}_s - m'\ddot{\mathbf{w}}, \tag{1}$$

where the (complex) elastic moduli in Biot's equations are calculated from the prescribed moduli as,

$$M = \frac{K_s}{1 - \frac{K}{K_s} + \Omega\left(\frac{K}{K_f} - 1\right)},$$

$$C = \frac{\left(1 - \frac{K}{K_s}\right)}{M},$$

$$H = \left(1 - \frac{K}{K_s}\right)C + K + \frac{4}{3}\mu, \tag{2}$$

and where $\mu = \mu_0(1 + \mathrm{i}\delta_\mu/\pi)$ is the complex shear modulus, μ_0 is the real part of μ, δ_μ is the log decrement of μ, K_f is bulk modulus of the fluid, K_s is the bulk modulus of the solid grains, $K = K_0(1 + \mathrm{i}\delta_K/\pi)$ is the complex bulk modulus of the solid frame, K_0 is the real part of K and δ_k is the log decrement of K.

Dots above a variable in equation (1) indicates a partial time-derivative. The $\exp(\mathrm{i}\omega t)$ time convention is applied, where ω is angle frequency and t is time. The parameter m' is defined as;

$$m' = \left(\frac{\rho_f}{\Omega}\right)\left[\alpha^2 - \frac{\mathrm{i}\eta\Omega F_v(\omega)}{\rho_f k_0\omega}\right], \tag{3}$$

where α is the tortuosity, $\eta = \rho_f v$ is the dynamic viscosity of the fluid, k_0 is the permeability and $F_v(\omega)$ is a frequency-dependent correction to the viscosity, which includes the pore size factor a [5].

Many of the Biot parameters are hard to determine or to measure directly. Fortunately, it turns out that just a few of the parameters have a significant effect on pulse propagation and particle velocities in the frequency range studied here. If only airborne pressure pulses are of interest, rigid-frame approximations will be sufficient in most cases [2]. In that case, permeability and depth of the porous layer will be most important. If ground particle velocities are of interest, bulk and shear moduli must also be included, and will be very important. These two parameters are directly related to the P- and S-wave speeds [19], which were measured as described in section 2. Some parameters (ρ_f, K_f and η) have table values, while some (K_s, K, μ and δ) were measured during the experiment [12]. Others (δ_f; a and α) turned out to have very little effect on waveforms and ground vibrations when they were varied within realistic ranges. They were thus given values assumed representative for the conditions studied. The sediment frame porosity, Ω, was measured to be in the range of 0·4–0·6, most probably close to 0·44 [12]. However, variation within these limits turned out to have ignorable influence on the results. Depth and permeability, k_0, of the poroelastic layer were assigned to different values listed in Tables 2 and 3. Shear

TABLE 3

List of cases discussed in the parameter study

Case	Depth of layer (m)	Permeability, k_0 (10^{-10} m^2)
A	0·1	100
B	0·1	10
C	0·1	1
D	0·3	100
E	0·3	10
F	0·3	1
G	0·5	100
H	0·5	10
I	0·5	1
J	1·0	100
K	1·0	10
L	1·0	1

and bulk attenuation is identical to those suggested by Attenborough *et al*. [20], since measured values for the site were not available. Results will be discussed in section 5. Shear and bulk moduli were assigned the values corresponding to the P- and S-waves listed for layer 1 and Table 1. Layers 2–6 were identical for the viscoelastic and poroelastic simulations. Finally, for the poroelastic simulations, a conversion factor of $2{\cdot}7 \times 10^4$ was applied, found by comparing the best-fit calculated overpressure amplitude and experimental data at 195 m from the source, in the same way as for the viscoelastic case.

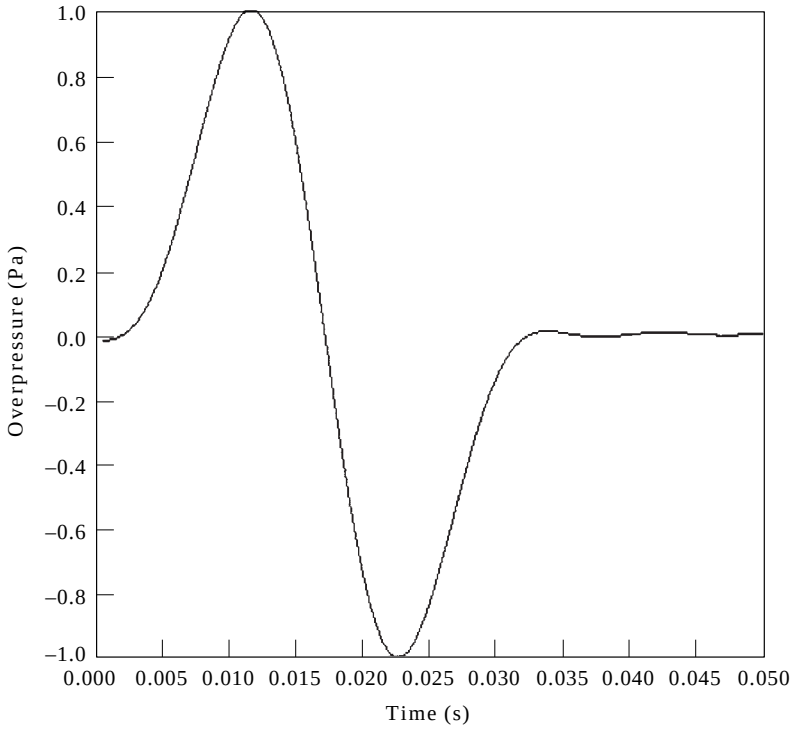

Figure 3. Normalized source pulse used in all FFP calculations.

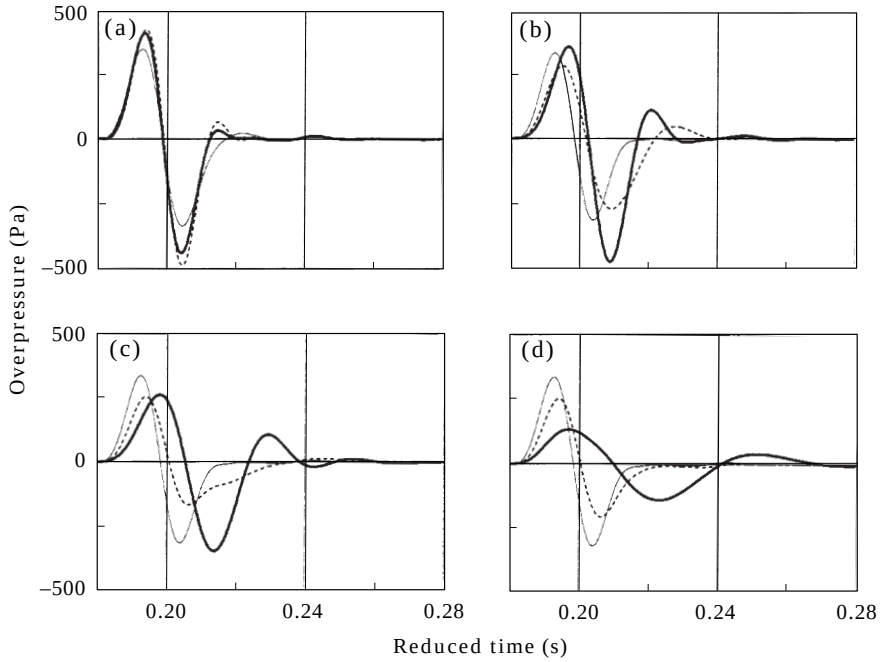

Figure 4. Overpressures at 195 m, predicted by poroelastic OASES. Receiver height is 2 m. Thin solid lines are $k_0 = 10^{-10}$ m^2, dashed lines are $k_0 = 10^{-9}$ m^2 and thick solid lines are $k_0 = 10^{-8}$ m^2. Depths of poroelastic layer are: (a) 0·1 m (Cases A, B and C); (b) 0·3 m (Cases D, E and F); (c) 0·5 m (Cases G, H and I); and (d) 1·0 m (Cases J, K and L).

4. MOVING-LOAD FORMULATION

A traditional approach to the prediction/simulation of ground vibration from airblasts has been through the *moving-load* formulation [21]. This approach is based on the observation that at large distances from a blast point, the air-pressure wave front propagates nearly horizontally over the ground surface and hence acts as a moving normal load. Although such models ignore atmospheric refraction, which in many cases has significant effect on the induced ground vibration, they nevertheless provide an effective means to gain insight into the mechanism of ground vibration and the interplay of the various environmental parameters. Use of this formulation in a similar study of simulation of blast-induced ground vibration produced satisfactory results [22].

In the realm of moving source mechanics, it has become customary to refer to the load speed as *subseismic*, *superseismic* or *transeismic*, depending on whether the load speed, c, is less than the shear wave velocity of the ground, V_s, greater than its compressional wave velocity, V_P, or is intermediate between these two velocities. Moreover, *Mach numbers* $M_s = c/V_s$ and $M_P = c/V_P$ have been defined to identify the load speed category.

As an airblast overpressure propagates over the ground its front approaches a plane surface at large distances. Therefore, in order to simulate the induced ground motions, one may adopt a 2-D plain-strain model of the ground perpendicular to the propagation direction. For constant propagation speed, c, in the x-direction, one can introduce a Fourier transform of the air pressure variation, $p(x, z, t)$, as

$$p(x, z, t) = \int \bar{p}(z)\, \mathrm{e}^{\mathrm{i}(-kx + \omega t)}\, \mathrm{d}\omega, \tag{4}$$

where $k = \omega/c$ is the wavenumber. Using the same time-space variation for the associated horizontal and vertical steady state ground displacements as

$$u(x, z, t) = \int \bar{u}(z)\, e^{i(-kx + \omega t)}\, d\omega, \tag{5}$$

$$v(x, z, t) = \int \bar{v}(z)\, e^{i(-kx + \omega t)}\, d\omega, \tag{6}$$

one can reduce the partial differential equations of wave propagation in a layered system to ordinary differential equations in terms of z. Solution of these equations in each layer and imposition of the appropriate boundary and interface conditions leads to the Fourier transformed values of u and v at layer interfaces. Space-time variation of ground motions can, then, be derived by the application of the inverse Fourier transform. More details on the solution scheme can be found in references [23–25]. It should be noted that this formulation is, in effect, a steady state solution as it assumes that the displacement field is moving with the load at the same speed. Therefore, it cannot represent those parts of induced ground motions that have another apparent propagation velocity.

5. EXPERIMENTAL AND THEORETICAL RESULTS

5.1. POROELASTIC AND VISCOELASTIC FFP PREDICTIONS

For the viscoelastic calculations, ground parameters shown in Table 1 were used. For the poroelastic calculations a fraction of the upper soil layer was replaced by one with poroelastic properties. This is a simplification, since the one top layer is made to represent

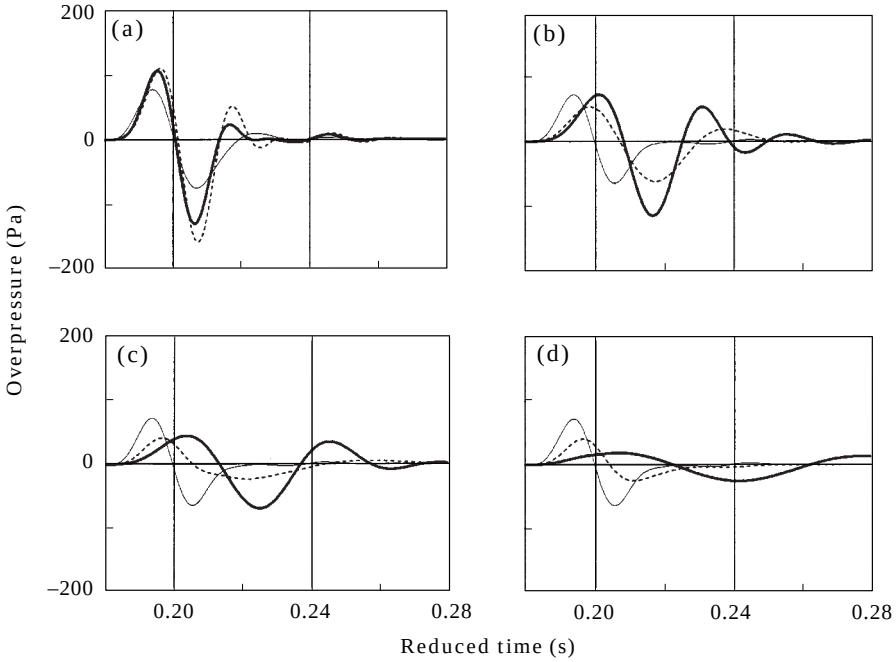

Figure 5. Same as Figure 4, but the range is 765 m.

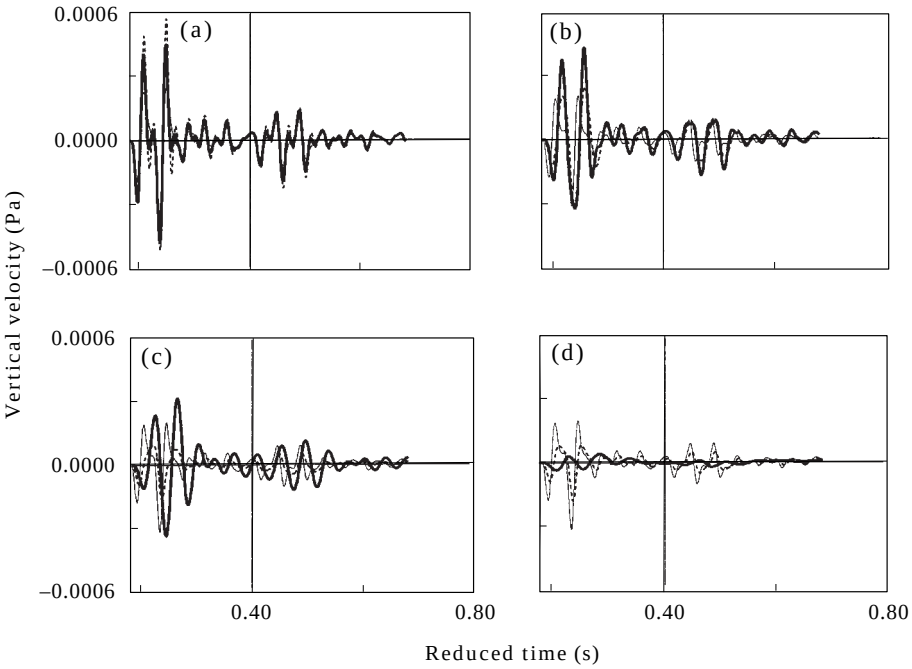

Figure 6. Same cases as Figure 5, but parameter is vertical ground surface velocity. Range is 765 m.

the real, more complex forest bed of moss, needles, sand and silt. Depth (thickness) and permeability of this top layer are assumed to be the two parameters most important for its behaviour and influence on the propagating airblast. They were subject to a parameter study as specified in Table 3. Figures 4 and 5 present typical results of the parameter study. They show computed air overpressure versus time 2 m above ground level at 195 and 765 m from the source, respectively. The time scale is "reduced" to start at zero at the onset of the signal, independent of the real arrival time. Each figure represents all three permeabilities in Table 3, for each layer thickness. It is clearly seen that both increased thickness and increased permeability decrease the peak pressure. It is further observed that for thin layers, the permeability does not affect the dominant frequency, while increased permeability tends to reduce the frequency for thicker poroelastic layers.

Figure 6 plots the corresponding computed vibration velocities of the ground surface at 765 m from the source. The same effects as for the pressure also appear for the velocities. Increased layer thickness and increased permeability decrease the peak velocity. As the layer thickness increases, the permeability tends to reduce more notably the dominant frequency of the vibrations.

Figure 7 compares the viscoelastic and poroelastic computed air pressures with those measured at 195, 260, 431 and 765 m from the source, respectively. The computed pressures from the poroelastic model belongs to Case G (Table 3), which gave the overall best match between the poroelastically computed and the measured air pressures. By examining the plots more thoroughly it is seen that the viscoelastic calculation gives the best match with the measurements at a short distance from the source, while the poroelastic gives the best match at longer distances. Particularly, the decrease in dominant frequency with increased distance, observed in the measurements, is perfectly simulated by the poroelastic calculations, but is not reproduced by the viscoelastic model.

Figure 8 makes a corresponding comparison of the ground vibration at the same distances, for Case G. It should be noted that for these ground conditions, the surface (and other) waves in the ground propagate more slowly than the air pressure wave, i.e., the situation is superseismic. By examining the plots it is seen that the peak ground velocities, in both measurements and calculations, appear as a direct response at the moment when the air pressure wave passes by. Generally, the poroelastic calculations overpredict this pressure peak. At short distances also the viscoelastic overpredicts the peak velocity, but it gives a reasonable match at longer distances. It should, however, be pointed out that other cases than G, which gave optimum match for the pressures, provided better match for the ground vibration. Case E was the one that gave the best match. Both the poroelastic and viscoelastic calculations reproduce the tail of ground vibrations following passage of the air pressure reasonably well. However, the poroelastic model gives the most realistic frequency characteristic of the ground vibration. The tail of oscillations was not produced when only the top ground layer was included in the calculations. The long oscillations observed here are a result of the ground layering.

The above observations may be summarized as in Figures 9–11. Figure 9 plots the decay of the peak (first positive) air pressure versus distance from the source, corresponding to Case G. The poroelastic case shown in G. This summary plot clearly shows that whereas both the viscoelastic and poroelastic model start from the same pressure at short distance, the poroelastic model gives a more realistic prediction of the pressure decay with increased distance. Figure 10 summarizes in the same way the maximum peak ground vibration. The figures shows that both models reproduce the right trend, but the viscoelastic model fits the measurements better than the poroelastic one (Case G). For other cases, such as E, there is a better match for the poroelastic model.

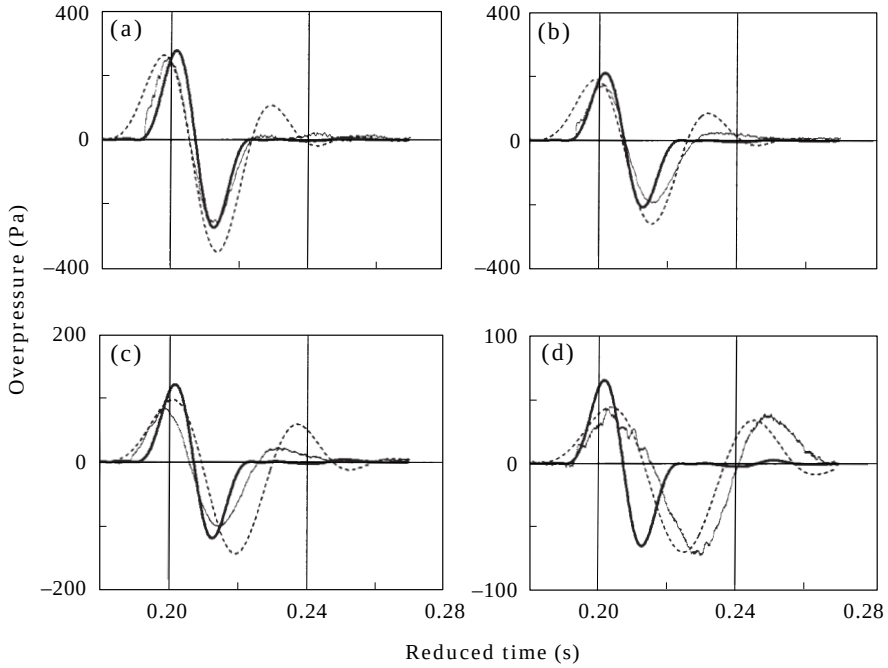

Figure 7. Comparison of viscoelastic OASES (——), poroelastic OASES (– – –, case G) and experimental data (——). Receiver height is 2 m. Ranges are: (a) 195 m; (b) 260 m; (c) 431 m; and (d) 765 m.

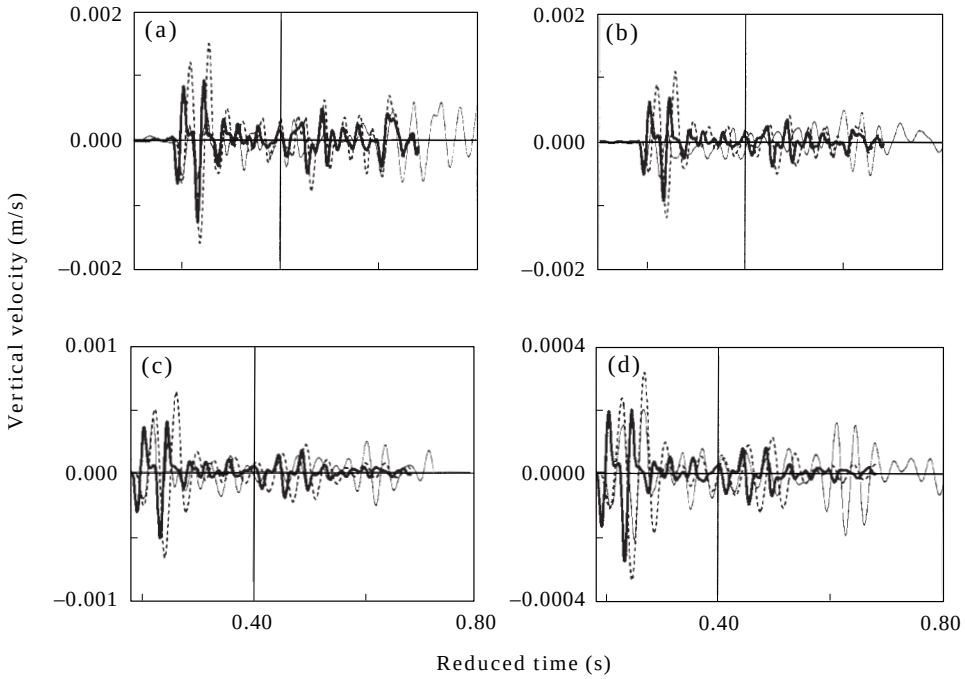

Figure 8. Same cases as Figure 7, but parameter is ground surface vertical velocity.

Figure 11 makes a very clear distinction between the viscoelastic and poroelastic results. The figure plots dominant frequency of the air pressure versus distance from the source. While the viscoelastic model predicts an almost constant frequency with distance, the poroelastic model gives a nearly complete match with the measured frequency decay with distance.

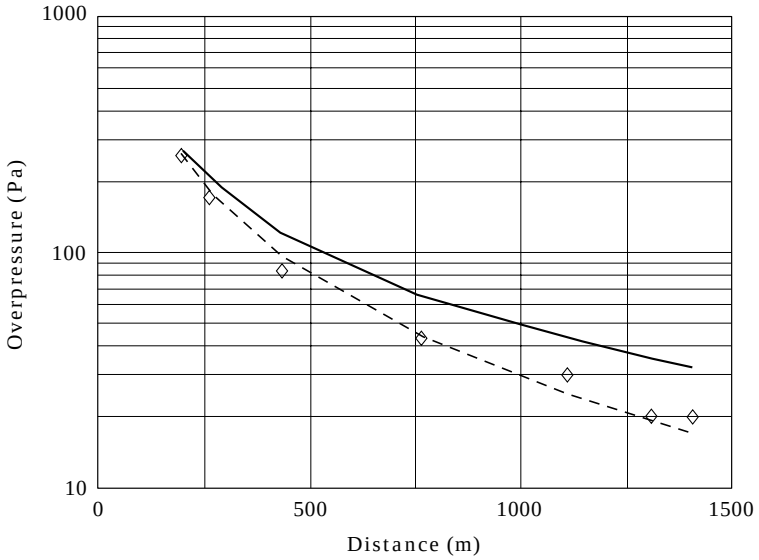

Figure 9. Decay of peak overpressure with distance from source for two OASES versions and experimental data. Receiver heights is 2 m. Peak is defined as the first arrival amplitude. ◇, Experiment; ——, viscoelastic; – – –, poroelastic.

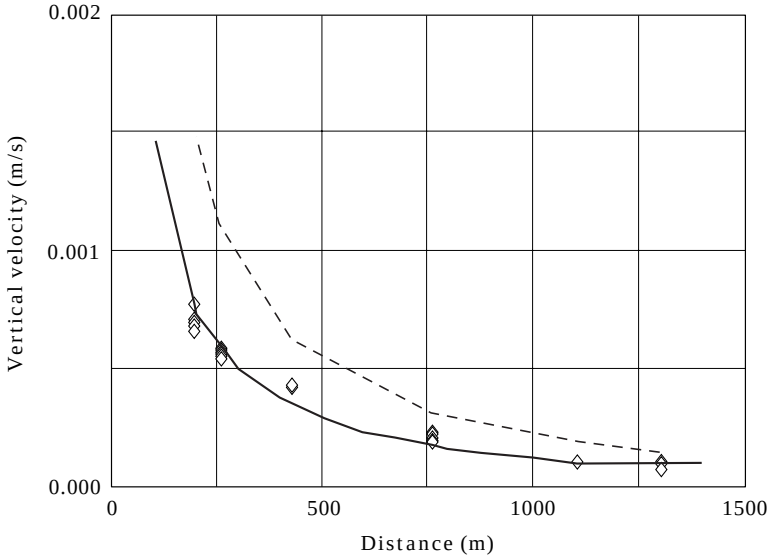

Figure 10. Same as Figure 9, but for peak vertical velocity.

5.2. PREDICTIONS OF GROUND VIBRATION BY THE MOVING-LOAD FORMULATION

Figure 12(a) shows the experimental and simulated ground vibration at 195 m from the blast. Ground parameters, as shown in Table 1, have been used. The moving source is the recorded overpressure at the same location. Comparison between the two time histories in this figure shows that whereas the peak values and the frequency characteristics of the vibrations are relatively well reproduced, the long tail of the observed motions is not well simulated. This could be expected as this part of vibration is, apparently, not a steady state propagating motion, with the same speed as the air pressure wave. In another case, when ground speeds were close to the speed of sound in air, ensuing motions were produced

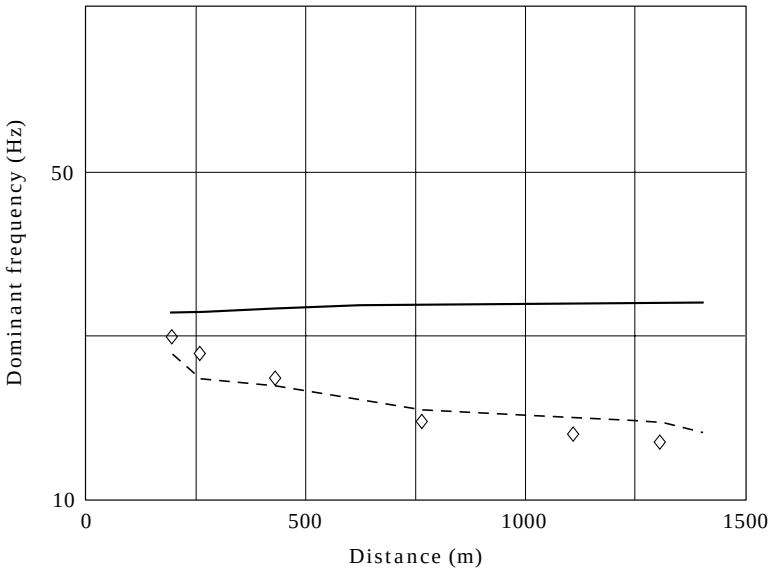

Figure 11. Same as Figure 9, but for dominant frequency of overpressure signal.

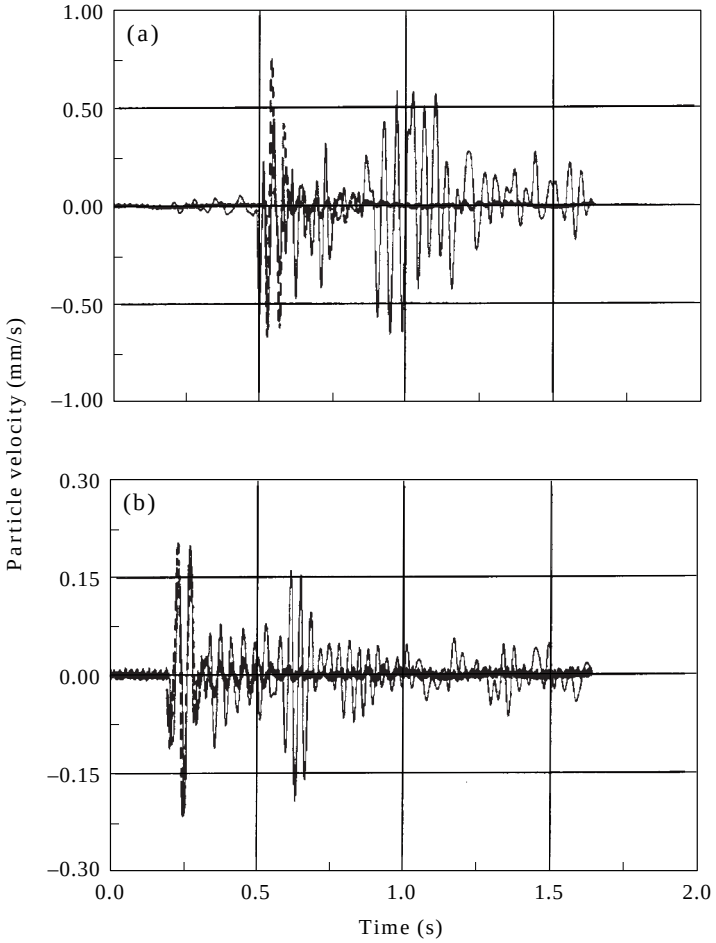

Figure 12. Comparison of *moving-load* simulation of ground surface vertical velocity and experimental data. Ranges are: (a) 195 m; and (b) 765 m. ——, measurement; – – –, simulation.

correctly by this model [22]. This could give the misleading conclusion that this approach generally handles all processes involved. The example presented here shows that the *moving-load* formulation has its limitations, particularly for the superseismic case.

Figure 12(b) displays a similar comparison for the ground particle velocity at 765 m from the blast. Even if a better match is observed between the measured and simulated motion at this distance (peak values within 10%), the simulation of the vibration tail is not yet satisfactory.

The above results suggest that the *moving-load* formulation may provide an efficient means to estimate the magnitude and frequency characteristics of blast-induced ground motions, e.g., for planning purposes. However, it has to be developed further to be able to represent the entire time variation of the vibration in a general case.

6. CONCLUDING REMARKS

This paper presented some experimental data of propagation of acoustic pulses out to a range of 1400 m along the ground. Both atmospheric overpressure and ground vibrations were measured. These data were compared with viscoelastic and poroelastic FFP

calculations. In the viscoelastic calculation, six ground layers were included, with the lower layer being a half-space. A fraction of the upper ground layer was then replaced with a poroelastic layer. Depth and permeability of this layer were varied, and the best values turned out to be 0·5 m and 10^{-8} m^2, respectively. In addition, the observed ground motion was compared with a *moving-load* simulation where the actual (experimental) overpressure was used as input. An homogeneous atmosphere was assumed in all calculations. The most important results turned out to be the following.

(1) Poroelastic predictions are most sensitive to depth and permeability of the poroelastic layer. (2) The observed airborne pulse approaches the poroelastic prediction as it propagates along the ground, even though a very simple model for the actual environment is applied. Both waveforms (dominant frequency) and peak amplitudes are well predicted. (3) Both versions of the FFP model give realistic values of the magnitude of the ground oscillations, but the viscoelastic version predicts too high frequency. (4) A *moving-load* simulation does not give a complete representation of all physical processes involved, even if a layered ground is included in the calculations. When the moving load propagates with a speed higher than the ground wavespeeds, (*superseismic* case), ensuing motions are not predicted. However, magnitude and frequency of the directly induced motion seems to be of correct size-order.

All data from the experiment presented here, and other experiments, are available in an open database. Information on this database can be found on the Internet site: www.bpof.inter.net.

ACKNOWLEDGMENTS

The authors are grateful to Henrik Schmidt at Massachusetts Institute of Technology for making the program OASES available to the research community, and to Arnfinn Jenssen at the Norwegian Defence Construction Service who initiated and managed the test program. This research was partly made possible by grants from the Norwegian Research Council, through *Strategic Institute Program*, SIP4.

REFERENCES

1. F. G. Don and A. J. Cramond 1987 *Journal of the Acoustical Society of America* **81**, 1341–1349. Impulse propagation in a neutral atmosphere.
2. D. G. Albert and A. Orcutt 1990 *Journal of the Acoustical Society of America* **87**, 93–100. Acoustic pulse propagation above grassland and snow: comparison of theoretical and experimental waveforms (and references therein).
3. L. R. Hole 1998 *Applied Acoustics* **53,** 77–94. An experimental and theoretical study of propagation of acoustic pulses in a strongly refracting atmosphere.
4. H. Schmidt 1997 *Massachusetts Institute of Technology*, *Department of Ocean Engineering*. OASES version 2.0; application and upgrades notes (and references therein).
5. N. P. Chotiros 1995 *Journal of the Acoustical Society of America* **97**, 199–214. Biot model of sound propagation in water-saturated sand.
6. S. Tooms, S. Taherzadeh and K. Attenorough 1993 *Journal of the Acoustical Society of America* **93**, 173–181. Sound propagation in a refracting fluid above a layered fluid-saturated porous elastic material.
7. H. Werkle and G. Waas 1987 *Soil Dynamics and Earthquake Engineering* **6**, 194–202. Analysis of ground motion caused by propagating air pressure waves.
8. G. Kerry 1996 *Inter-noise* **96,** 583–588. An overview of the long range impulse sound propagation measurements made in Norway.
9. L. R. Hole and R. L. Guice 1997 *5th Congress on Sound and Vibration*, *University of Adelaide*, *Australia*. An open database on propagation of low frequency impulse noise in the atmosphere. And references therein.

10. L. R. Hole, P. Lunde and Y. Gjessing 1997 *Journal of the Acoustical Society of America* **102,** 1443–1453. Effects of strong sound velocity gradients on propagation of low frequency impulse noise; comparison of FFP predictions and experimental data.
11. R. Ford, D. J. Saunders and G. Kerry 1993 *Journal of the Acoustical Society of America* **94**, 408–417. The acoustic pressure waveform from small unconfined charges of plastic explosive.
12. C. Madshus 1995 *NGI Report* 515137-1. Blast propagation through forest—NOR94/2 Tests.
13. A. M. Kaynia and C. Madshus 1995 *Norwegian Geotechnical Institute*, *NGI report* 515137-4. Blast propagation through forest—NOR95/1 tests.
14. K. H. Stokoe, G. R. Rix and S. Nazarian 1989 12*th International Conference on Soil Mechanics and Foundation Engineering* **1**, 331–334, Riode Janeiro, Brazil. In situ seismic testing of surface waves.
15. L. R. Hole, Y. Gjessing, T. de Lange and J. W. Reed 1998 *Noise Control Engineering Journal*. Meteorological measurements and conditions during Norwegian trials (in press).
16. H. Schmidt 1987 *Report no*. *SR*-113, *SACLANTCEN Research Centre*, *La Spezia*, *Italy*. SAFARI, Seismo-acoustic fast field algorithm for range-independent environments; users guide.
17. M. A. Biot 1956 *Journal of the Acoustical Society of America* **28**, 168–178. Theory of propagation of elastic waves in a fluid-saturated porous solid, I. Low-frequency range.
18. M. A. Biot 1956 *Journal of the Acoustical Society of America* **28**, 179–191. Theory of propagation of elastic waves in a fluid-saturated porous solid, II. Higher frequency range.
19. R. D. Stoll and G. M. Bryan 1970 *Journal of the Acoustical Society of America* **47**, 1440–1447. Wave attenuation in saturated sediments.
20. K. Attenborough, S. Taherzadeh, H. E. Bass, R. Raspet, G. R. Becker, A. Güdesen, A. Chrestman, G. A. Daigle, A. L'Espérance, Y. Gabillet, K. E. Gilbert, Y. L. Li, M. J. White, P. Naz, J. M. Noble and H. A. J. M. Van Hof 1995 *Journal of the Acoustical Society of America* **97**, 173–191. Benchmark cases for outdoor sound propagation models.
21. J. W. Miles 1960 *Journal of Applied Mechanics* **27**, 710–716. On the response of an elastic half-space to a moving blast wave.
22. C. Madshus and A. M. Kaynia 1997 *NGI Report* 515155-1. Ground response to propagating airblast.
23. E. Kausel and J. M. Roësset 1981 *Bulletin of the Seismological Society of America* **71**, 1743–1761. Stiffness matrices for layered soils.
24. R. Siddharthan, Z. Zafir and G. Norris 1993 *Journal of Engineering Mechanics*, *ASCE* **119**, 2052–2071. Moving load response of layered soil. I: formulation.
25. C. Montcourt 1995 *NGI Report* 515146-1. Propagating shocks and moving loads on ground—two dimensional theoretical solutions.